

ELECTRONIC SUPPORTING INFORMATION

An *in situ* spectroelectrochemical study on the orientation changes of an [Fe^{III}L^{N2O3}] metallosurfactant deposited as LB Films on gold electrode surfaces

Izabella Brand,^{a,*} Joanna Juhaniewicz-Debinska,^b Lanka Wickramasinghe,^c and Claudio N. Verani,^{*,c}

Contents:

SI.1 Langmuir monolayers of [Fe^{III}L^{N2O3}] molecules.

Figure S1. Langmuir monolayer of **1** at the air|water interface. Inset: compressibility modulus (K_s) vs. area per molecule plot.

SI. 2 Capacitance of [Fe^{III}L^{N2O3}] in LB monolayer and 5LB films.

Figure S2. Capacitance vs. potential curves of **1** in LB films on the Au electrode surface: (a) monolayer and (b) 5 LB film; thin dotted line – unmodified Au electrode, 1 – first negative, 2 – successive positive, 3 – successive negative going potential scans.

SI.3 Isotropic optical constants of [Fe^{III}L^{N2O3}].

Figure S3. The refractive index (dashed line) (n) and attenuation coefficient (solid line) (k) of **1** in (a) 3100-2700 and (b) 1700-1150 cm⁻¹ spectral regions.

SI.4. Deconvolution of the PM IRRA spectra of [Fe^{III}L^{N2O3}] in CH stretching modes region.

Figure S4. Deconvolution of the PM IRRA spectra in the CH stretching modes region of the LB monolayer of **1** on Au surface at (a) $E = -0.3$ V and (b) $E = -0.8$ V.

SI.5. PM IRRA spectra of [Fe^{III}L^{N2O3}] in LB films in ring stretching modes region.

Figure S5. PM IRRA spectra in 1680 – 1330 cm⁻¹ spectral region of (a) randomly distributed **1** molecules in a 1-LB thick film; and in the monolayer of **1** on the Au electrode surface in (b) first negative, (c) subsequent positive and (d) subsequent negative potential scans at indicated potentials.

Figure S6. PM IRRA spectra in 1680 – 1330 cm⁻¹ spectral region of (a) randomly distributed **1** molecules in a 5-LB thick film and in 5-LB film of **1** on the Au electrode surface in (b) first negative and (c) subsequent positive going potential scans at indicated potentials.

SI.1 Langmuir monolayers of [Fe^{III}L^{N2O3}] molecules. The Langmuir monolayer of the studied metallosurfactant [Fe^{III}L^{N2O3}], **1**, at the air|water interface is shown in **Figure S1**. First, **1** was dissolved in chloroform to give the concentration of metallosurfactant of 1 mg mL⁻¹. Few μ L of **1** was placed at air|water interface in the Langmuir trough (KSV, Helsinki, Finland). Using symmetric barriers the monolayer was compressed at the speed of barrier movement set to 10 mm min⁻¹. The Langmuir isotherm of **1** at the air|water interface is shown in **Figure S1**. The surface pressure starts to increase slowly below the lift-off area (2.3 nm²). At the surface pressure of 20 – 25 mN m⁻¹ and corresponding area per molecule range of 1.4 – 1.0 nm² a discontinuity on the isotherm is observed. After this transition the surface pressure increases to 55 – 60 mN m⁻¹. The monolayer collapses at the average area per molecule of 0.64 \pm 0.04 nm².

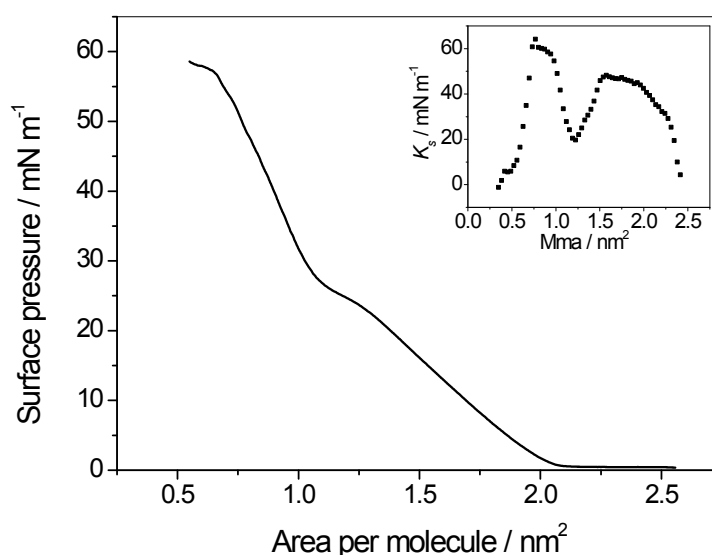


Figure S1. Langmuir monolayer of **1** at the air|water interface. Inset: compressibility modulus (K_s) vs. area per molecule plot.

The compressibility modulus (K_s) of the monolayer was calculated using the following equation ^{1,2}:

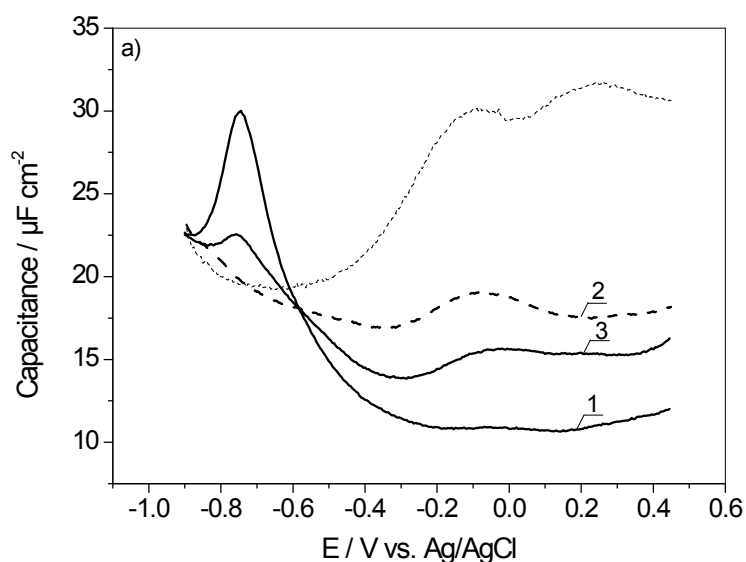
$$K_s = \left[- \left(\frac{1}{A} \right) \left(\frac{dA}{d\pi} \right) \right]^{-1} \quad (1),$$

where A is the area per molecule in the monolayer at a given surface pressure π . K_s values are useful for the characterization of the physical state of the monolayer; in the liquid expanded (disordered) (LE) state they vary from 12.5 to 50 mN m⁻¹, in the liquid condensed (ordered) (LC) from 100 to 250 mN m⁻¹. A transition to a solid phase (S) results in an increase in the K_s values up to 2000 mN m⁻¹.² Before the phase transition in the monolayer, at $A < 1.5$ nm², K_s reaches a maximum of 46 – 47 mN m⁻¹. Upon the transition, at $A > 1.0$ nm² K_s values increase to 60 mN m⁻¹. The inset to **Figure S1** shows

clearly that the monolayer of **1** exists in a liquid state. The discontinuity in the isotherm corresponds to some rearrangements in the monolayer and not to a change in the physical state of **1** in the monolayer.

SI. 2 Capacitance of [Fe^{III}L^{N2O3}] in LB monolayer and 5LB films. Electrochemical measurements were performed in an all-glass three-electrode cell with either a polycrystalline Au disc electrode or an evaporated gold film on glass as the working electrode. A gold wire served as the counter electrode and a Ag|AgCl|sat.KCl (Ag|AgCl) as the reference electrode. A CHI660A potentiostat (CH Instruments, Austin, USA) with the corresponding software was used to perform the electrochemical measurements. The AC voltammograms were recorded in positive and negative directions with a scan rate of 5 mV s⁻¹ and an AC perturbation with 10 mV amplitude and 20 Hz frequency. The capacitance vs. potential curve was calculated assuming the cell being equivalent to a resistor in series with a capacitor from the in-phase and out-of-phase components of the signal.

Figure S2 shows the capacitance vs. potential curves of **1** in 1LB and 5 LB films on the Au electrode surface.



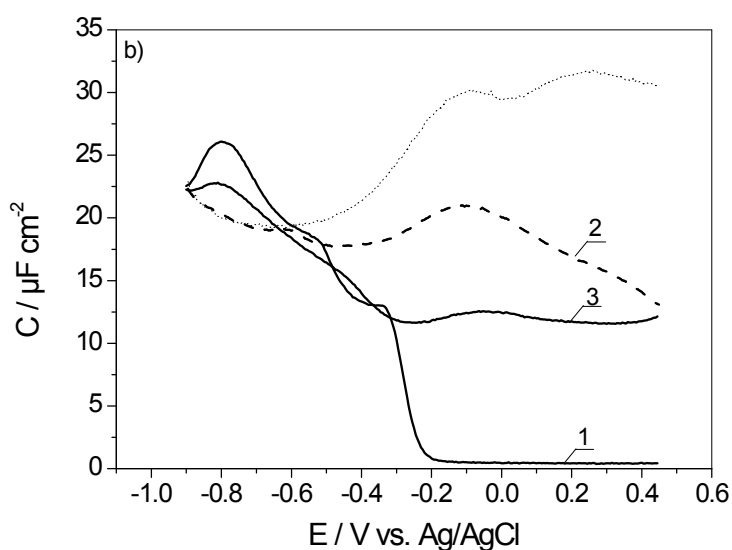


Figure S2. Capacitance vs. potential curves of **1** in LB films on the Au electrode surface: (a) monolayer and (b) 5 LB film; thin dotted line – unmodified Au electrode, 1 – first negative, 2 – successive positive, 3 – successive negative going potential scans.

In the first negative going potential scan the capacitance-potential curves of **1** in LB films have a distinct characteristic. Before reduction at $E < -0.3$ V, the capacitance of LB films of **1** has a minimal value ($10\text{--}11 \mu\text{F cm}^{-2}$ and $0.35 \mu\text{F cm}^{-2}$ in 1LB and 5LB films, respectively). Reduction reaction is accompanied by a significant increase (to ca. $13\text{--}18 \mu\text{F cm}^{-2}$) in the capacitance of the Au surface modified with LB films. These curves show also that **1** in the reduced state remains adsorbed on the metal surface. The potential-driven desorption occurs at $E = -0.74$ V and $E = -0.79$ V in the monolayer and 5LB film, respectively. Reverse of the potential scan leads to a resorption of **1** on the Au surface. A loss of redox-activity the re-adsorbed molecules of **1** in LB films is characterized by a higher capacitance, indicating some changes in the film structure and / or composition.

SI.3 Isotropic optical constants of $[\text{Fe}^{\text{III}}\text{L}^{\text{N}2\text{O}3}]$. The optical constants of **1** were determined from a transmission IRS measurement of solution spectra of the compounds dissolved in CCl_4 as the solvent using well established procedure.^{3, 4} A Kramer-Kroenig transformation was used to determine the attenuation coefficient (k) and the refractive index (n) of the studied molecule in $3100 - 2800 \text{ cm}^{-1}$ (CH stretching modes region) and in $1800 - 1000 \text{ cm}^{-1}$ (CC and CO stretching modes at aromatic and phenyl groups, respectively) spectral regions. The isotropic optical constants are shown in **Figure S3**.

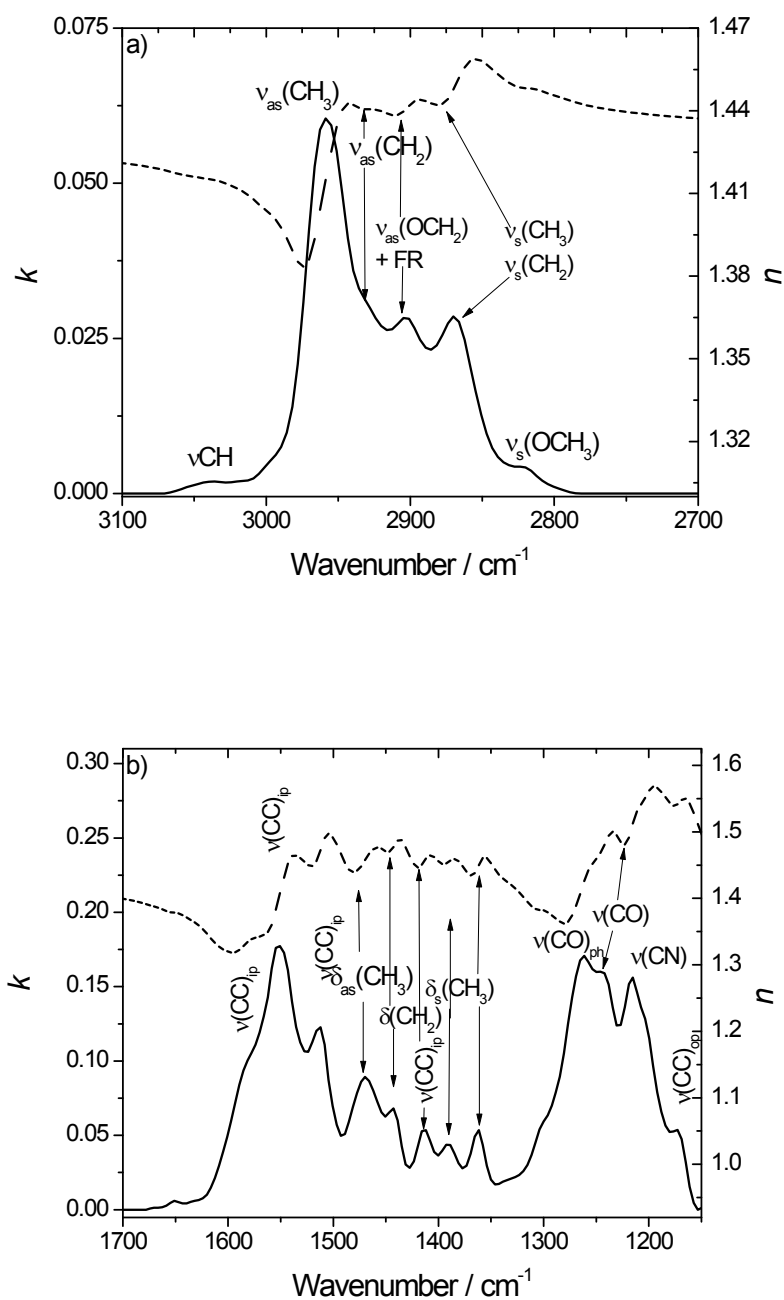


Figure S3. The refractive index (dashed line) (n) and attenuation coefficient (solid line) (k) of **1** in (a) 3100-2700 and (b) 1700-1150 cm^{-1} spectral regions.

SI.4. Deconvolution of the PM IRRA spectra of $[\text{Fe}^{\text{III}}\text{L}^{\text{N}2\text{O}3}]$ in CH stretching modes region. In order to deconvolute the PM IRRA spectra of **1** in LB films on the Au electrode surface the second derivative of each spectrum was calculated. In this way the number and frequency of individual IR absorption modes in the analyzed spectrum were found. Next, a mixed Gauss-Lorentz fit procedure was used to deconvolute individual modes. The number of IR absorption modes in the PM IRRA spectra of **1** in LB films depends on the potential applied to the Au electrode surface. **Figure S4** shows deconvolution of

the PM IRRA spectra in the monolayer of **1** on the Au surface at $E = -0.3$ V (monolayer adsorbed on the electrode surface) and $E = -0.8$ V vs. Ag/AgCl (desorbed monolayer).

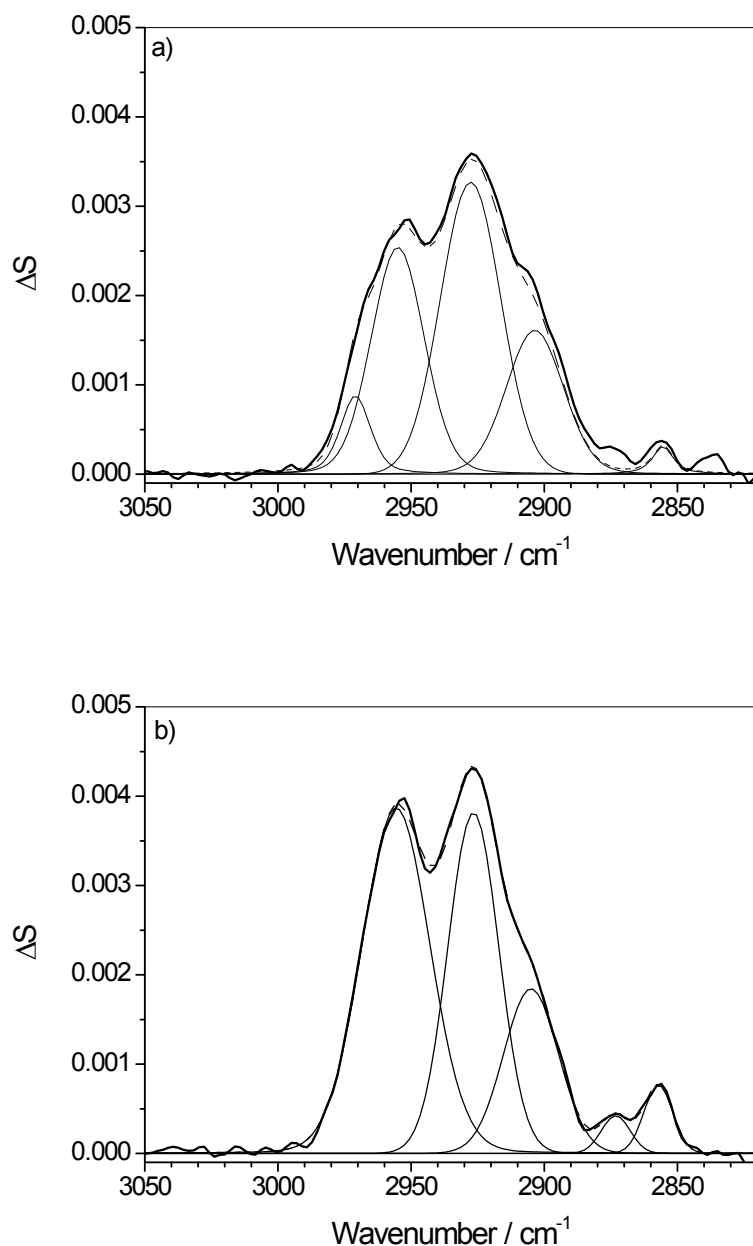


Figure S4. Deconvolution of the PM IRRA spectra in the CH stretching modes region of the LB monolayer of **1** on Au surface at (a) $E = -0.3$ V and (b) $E = -0.8$ V.

SI.5. PM IRRA spectra of $[\text{Fe}^{\text{III}}\text{L}^{\text{N}203}]$ in LB films in ring stretching modes region. Figures S5 and S6 show the PM IRRA spectra of the LB films of **1** in the $1700 - 1300$ cm^{-1} spectral region. This spectral region shows IR absorption bands arising from in-plane stretches of the aromatic rings as well as methyl and methylene deformation modes. The thick lines in Figures S5 and S6 show the IR spectra

of the monolayer and the 5-layer LB film calculated from isotropic optical constants corresponding to a random distribution of molecules of **1** in these films.

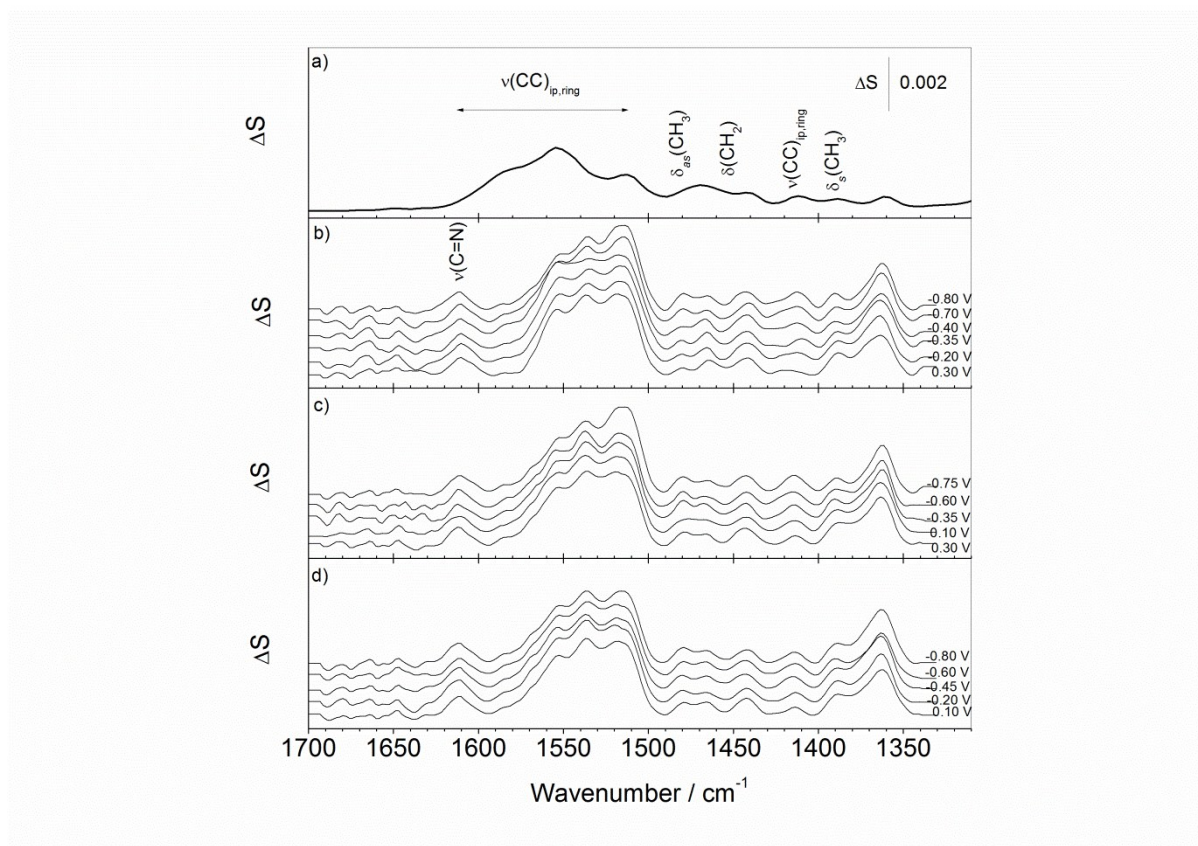


Figure S5. PM IRRA spectra in 1680 – 1330 cm^{-1} spectral region of (a) randomly distributed **1** molecules in a 1-LB thick film; and in the monolayer of **1** on the Au electrode surface in (b) first negative, (c) subsequent positive and (d) subsequent negative potential scans at indicated potentials.

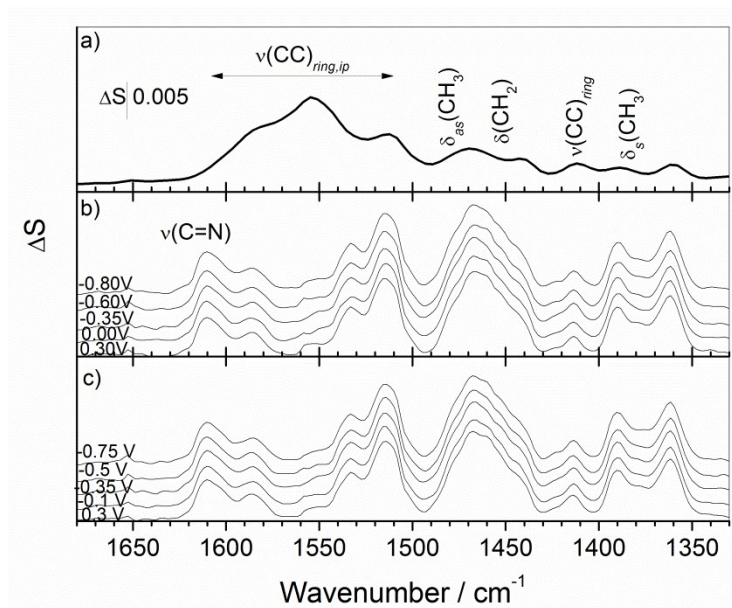


Figure S6. PM IRRA spectra in 1680 – 1330 cm^{-1} spectral region of (a) randomly distributed **1** molecules in a 5-LB thick film and in 5-LB film of **1** on the Au electrode surface in (b) first negative and (c) subsequent positive going potential scans at indicated potentials.

As shown in **Figures S5** and **S6** in the IR spectra of randomly distributed molecules the aromatic rings give rise to four in-plane stretching modes. Their maxima of absorption appear at $1585.4 \pm 0.2 \text{ cm}^{-1}$, $1551.7 \pm 0.2 \text{ cm}^{-1}$; $1512.5 \pm 0.2 \text{ cm}^{-1}$ and $1411.9 \pm 0.2 \text{ cm}^{-1}$. In the liquid state of **1** the two high frequency modes of the in-plane ring stretching modes in the aromatic rings are broad. Because the four aromatic rings present in **1** differ in chemical environment, any or all four may have overlapping contributions broadening their in-plane stretching modes. The $\delta_{as}(\text{CH}_3)$ and $\delta(\text{CH}_2)$ modes appear between 1470 and 1440 cm^{-1} . The symmetric $\delta_s(\text{CH}_3)$ mode is split into two bands centered at 1389.0 and 1360.2 cm^{-1} . They arise from an umbrella mode: a simultaneous out-of-plane and in-plane symmetric deformation mode at a methyl group.⁵ Two new bands appear in *in situ* PM-IRRA spectra of LB films (**Figures S5, S6**). A band at $1609.4 \pm 0.3 \text{ cm}^{-1}$ arises from the $\nu(\text{C}=\text{N})$ stretching group at the imine group, as a consequence of oxidation of the amine group of **1** at the air|water surface.⁶ In LB films of **1**, the in-plane ring stretching modes have well-resolved absorption modes centered at: 1585, 1555, 1535, 1512 and 1414 cm^{-1} . In the PM IRRA spectra of LB films a new absorption band at 1535 cm^{-1} is clearly visible (**Figures S5, S6**). Narrowing and connected with it increased resolution of the overlapped IR absorption modes point on a long-range molecular scale order in rigid LB films.

Compared to the spectra of randomly distributed molecules, the intensities of some IR absorption modes in the LB films are demonstrably enhanced while others are attenuated (**Figures S5,S6**). In the monolayer of **1**, the modes at 1585 cm^{-1} and 1555 cm^{-1} are attenuated while the intensities of the modes centered at 1535 cm^{-1} , 1512, 1440-1455, 1414, and $1380\text{-}1360 \text{ cm}^{-1}$ are enhanced (**Figure S5**).

More extensive spectral changes are detected in the multilayer film (**Figure S5**); the in-plane ring stretching modes at 1587, 1555 and 1535 cm^{-1} are attenuated while the modes with at 1512, 1414 as well as the $\delta(\text{CH}_2)$ and $\delta_s(\text{CH}_3)$ modes are enhanced. Therefore, it appears that there is a well-defined molecular orientation in LB films of **1**. Interestingly, applied potentials have negligible effect on this spectral region. The transition dipole vectors of the in-plane stretching rings ($\nu(\text{CC})$) are located within the plane of the ring. Because the four aromatic rings present in **1** have different orientations within the molecule the quantitative analysis of ring orientation was not performed. In both LB films the attenuation of ring stretching modes at 1587, 1555 cm^{-1} suggests that the planes of the four aromatic rings tend to orient themselves parallel to the Au surface. Neither the reduction of **1** ($E < -0.3$ V) nor its potential driven desorption from the surface (at $E < -0.75$ V) influence this arrangement. However, in the monolayer, at $E < -0.3$ V, a small increase in the intensities of the ($\nu(\text{CC})_{\text{b}}$) modes at 1512 and 1414 cm^{-1} is observed. It might be tentatively associated with the reorientation of a detached ring resulting from the $\text{Fe}^{\text{III}}/\text{Fe}^{\text{II}}$ reduction.

References:

1. R. Almog and C. A. Mannella, *Biophys. J.*, 1996, 71, 3311-3319.
2. J. M. Smaby, M. Momsen, V. S. Kulkarni and R. E. Brown, *Biochemistry*, 1996, 35, 5696-5704.
3. D. L. Allara, A. Baca and C. A. Pryde, *Macromolecules*, 1978, 11, 1215-1220.
4. V. Zamlynny and J. Lipkowski, in *Adv. Electrochem. Sci. Eng.*, eds. R. C. Alkire, D. M. Kolb, J. Lipkowski and P. N. Ross, Wiley-VCH, Weinheim, Editon edn., 2006, vol. 9, pp. 315-376.
5. D. Sajan, K. P. Laladhas, I. Hubert Joe and V. S. Jayakumar, *J. Raman Spectrosc.*, 2005, 36, 1001-1011.
6. L. D. Wickramasinghe, M. M. Perera, L. Li, G. Mao, Z. Zhou and C. N. Verani, *Angew. Chem. Int. Ed.*, 2013, 52, 13346-13350.